

High-quality Brewster's angle polarizer for broadband infrared application

Daniel J. Dummer, Simon G. Kaplan, Leonard M. Hanssen, Alan S. Pine, and Yugin Zong

We have designed and constructed a linear polarizer for use with visible and infrared radiation. The broadband polarizer consists of four germanium plates arranged in a chevron geometry. Input radiation is incident near Brewster's angle for the first plate such that the reflected beam is preferentially *s*-wave polarized. This reflected beam is steered subsequently to the successive plates, always intersecting near Brewster's angle. The beam polarization at the output of the device is almost completely *s*-wave polarized. The ratio of the paraxial flux of the nearly extinguished *p*-wave polarized light to the *s*-wave polarized light transmitted through the device is found to be less than 10^{-5} for laser illumination at wavelengths of 0.633, 1.32, 3.39, and 10.6 μm . Calculations predict that extinction ratios less than 10^{-5} are achievable over the wavelength range from 0.4 μm to beyond 500 μm . Alternative design geometries involving fewer plates are also described along with their advantages and disadvantages.

OCIS codes: 230.5440, 260.3060, 260.5430.

1. Introduction

High-quality linear polarizers spanning visible and infrared wavelengths are generally not available. Applications for broadband linear polarizers include optical polarimetry, which can more completely characterize optical materials than transmittance and reflectance measurements, especially for anisotropic materials. We have been developing polarization-resolved transmittance and reflectance measurement capabilities over a broad spectral range including visible and infrared wavelengths. Our primary purpose for optical polarimetry is calibrating optical polarization components. We use Fourier-transform spectrometers over the wavelength range from 1 to 30 μm and prism- and grating-based spectrometers over the wavelength range from 0.190 to 28 μm . We also use lasers at various wavelengths within this range. Specifically, polarization metrology is under development for wavelengths less than 5 μm . For polarization metrology, we employ high-performance chevron geometry Brewster's angle polarizers.¹⁻⁴ These germanium-reflective polariz-

ers are designed to operate over a broad wavelength range, including the visible and infrared spectrum.

In this paper we discuss the design, construction, and performance of chevron geometry polarizers. In this section we define the pertinent performance characteristics of the polarizers. In Section 2 we discuss the wavelength range and extinction performance of various types of polarizers. In Section 3 we discuss device design and construction of the chevron geometry germanium polarizers. In Section 4 we describe the testing of the devices with laser light at four wavelengths. In Section 5 we discuss the performance of the polarizers, and in Section 6 we summarize the paper.

Real optical polarizers do not completely extinguish the unwanted polarization component. A useful performance parameter for linear polarizers is the extinction ratio ρ , defined⁵ as the ratio k_2/k_1 of the minimum transmittance k_2 to the maximum transmittance k_1 for linearly polarized incident light.⁶ See Appendix A for further discussion of this definition. When referring to the extinction ratio ρ , less is better. We refer to the minimum transmittance k_2 and the maximum transmittance k_1 as the minor and major principal transmittances of the polarizers, respectively. The principal transmittances of polarizers depend on wavelength, often dramatically. To perform polarization component calibrations, we want master polarizers with extremely low extinction ratios. In addition to the extinction ratio ρ and the

The authors are with the National Institute of Standards and Technology, Optical Technology Division, Gaithersburg, Maryland 20899.

Received 23 June 1997; revised manuscript received 14 October 1997.

major principal transmittance k_1 , other polarizer performance parameters are also important. These include optical beam displacement, optical beam angular deviation, sensitivity to beam convergence⁷ and input angle, sensitivity to input power level, and generation of multiple beams. We require that the polarizers should be easy to use and align. Because we mount them on motorized rotation stages for repeated mechanical rotations, the polarizers must also be robust and rugged.

2. Performance Overview of Various Polarizer Types

Most linear polarizers are of one of the following types: (a) dichroic polarizers, (b) wire grid polarizers, (c) anisotropic crystal polarizers, (d) transmissive, or (e) reflective Brewster's angle polarizers. The performance varies for each type because of the different underlying polarization mechanisms. Each type is described below. We assessed each for possible metrology application.

A. Dichroic Polarizers

Dichroic polarizers rely on anisotropic absorption. These may consist of oriented polymers, oriented metal particles, or anisotropic single crystals. For research at visible wavelengths, a sheet of oriented, dyed polymer preferentially absorbs light polarized along one direction. Extinction ratios are typically of the order of $\rho \sim 10^{-3}$ over the specified wavelength range. A typical usable wavelength range is from 400 to 800 nm for the dichroic sheet polarizers (although some are available from 900 to 2000 nm). The major principal transmittance k_1 is typically 0.6 over the specified wavelength range. Dichroic sheet polarizers can have a large acceptance angle, exceeding 500 mrad.

For research in the near infrared, small needle-shaped silver particles oriented within a glass host slab⁸ preferentially absorb polarized light. A typical version of these polarizers is optimized at 1330 nm with an extinction ratio ρ less than 10^{-5} . These have a fairly narrow wavelength range of utility, between 900 and 1700 nm in which the extinction ratio is less than 10^{-2} . The major principal transmittance k_1 is approximately 0.9 over the narrow specified wavelength range. As with the dichroic sheet polarizers, they are expected to have a large acceptance angle.

For research at very specialized wavelengths, particular anisotropic crystals can be used. Resonant absorption can occur for electric-field vibrations along a particular crystallographic axis. For example, calcite has strong anisotropic absorption at 3.4 and 3.9 μm over a 0.1- μm bandwidth. The extinction ratio ρ can be 2×10^{-8} to 1×10^{-9} at 3.39 μm .⁹ We used a dichroic calcite polarizer for our 3.39- μm wavelength He-Ne laser measurements. The major principal transmittance k_1 in the anisotropic absorption band is approximately 0.73, depending on the thickness. Crystallographic constraints restrict the acceptance angle.

These three dichroic polarizers exhibit minimal

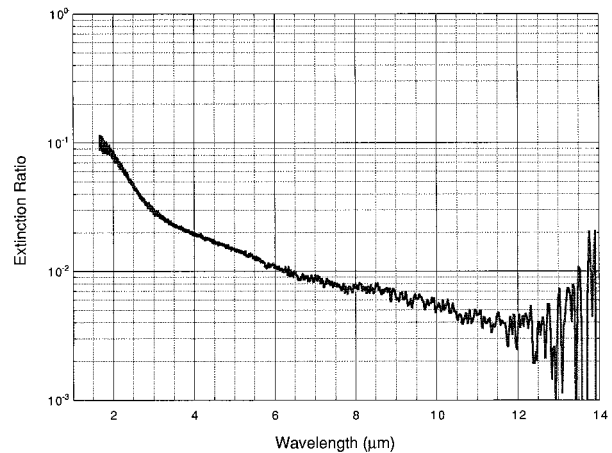


Fig. 1. Extinction ratio versus wavelength of an infrared wire grid polarizer as measured with a Fourier-transform spectrometer. The wire grid polarizer consists of gold lines patterned with a 0.25- μm period on a barium fluoride substrate.

beam deviation and beam displacement because of their thin-slab construction. Because the dichroic polarizers absorb light of the unwanted polarization state, heating can be a problem in high-power applications. But because it is absorbed rather than reflected, stray light of the unwanted polarization state is advantageously quenched. Primarily because of the limited wavelength ranges, dichroic polarizers do not meet our needs for polarization metrology over a broad spectral range.

B. Wire Grid Polarizers

Wire grid polarizers consist of parallel metallic lines in a jail bar pattern and achieve their polarizing properties through anisotropic conduction. In contrast to the anisotropic absorption of dichroic polarizers, the light polarized with the electric field along the wire direction is preferentially reflected; the orthogonally polarized light is preferentially transmitted. The wavelength scale over which a wire grid device functions is set by the wire size and spacing. At large wavelengths compared to the spacing, the polarizer acts as an ideal anisotropic sheet conductor, but as the wavelength decreases and approaches the wire spacing, higher-order spatial modes are excited and the extinction ratio increases. This effect is demonstrated in Fig. 1, which shows the spectral extinction ratio for a typical commercial wire grid polarizer consisting of 0.25- μm Au wires on a BaF_2 substrate. Extinction ratios can be less than 10^{-3} for long wavelengths but usually exceed 10^{-2} for wavelengths less than 5 μm . The major principal transmittance is limited by the substrate and is typically in the range of 0.5 to 0.9, although free-standing wire grids can be used for sufficiently long wavelengths. Acceptance angles can be greater than 100 mrad, and beam deviation and displacement are low because of the slab geometry of the substrate. However, because of their generally poor performance at short infrared wavelengths, wire grid

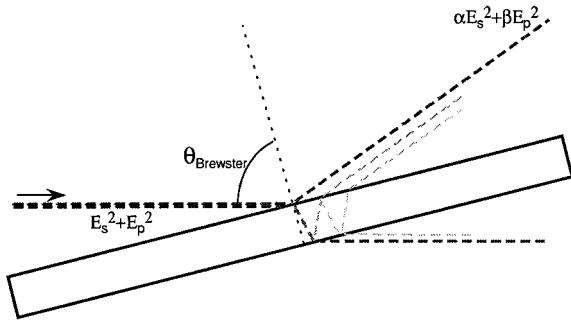


Fig. 2. Idealized detail of the radiation impinging on a dielectric plate. The primary, first-surface reflected beam and the primary refracted beam are represented by the darker dashed lines. The lighter dashed lines show the first few secondary beams resulting from second-surface reflections. These secondary beams become continually lighter. When the angle of incidence is near Brewster's angle, the reflected radiation is almost entirely *s*-wave polarized.

polarizers are not suitable as master polarizers for broadband polarization metrology.

C. Anisotropic Crystal Polarizers

Anisotropic crystal polarizers consist of prisms of birefringent crystals oriented such that the ordinary ray and the extraordinary ray are steered away from one another, allowing the unwanted polarization component to be dumped. The most common types use calcite crystals in a Glan or Wollaston configuration. Extinction ratios less than 10^{-5} are not uncommon over a spectral range from 300 to 2200 nm, and the major principal transmittance k_1 is approximately 0.8 over this wavelength range. However, acceptance angles are low, typically 50 mrad; beam deviation may be 1 mrad or greater; and beam displacement can be large for large angles of incidence, making these polarizers difficult to use in a rotating mode because the transmitted beam can move significantly on the detector. As with other transmissive polarizers, front and back surface interreflections generate multiple beams. Although the performance is high at ultraviolet, visible, and near-infrared wavelengths, calcite Glan polarizers are not applicable for longer infrared wavelengths. Other anisotropic materials (e.g., AgGaS₂) could in principle be used at longer wavelengths, but are expensive and not readily available, and in any case would not extend beyond approximately 10 μm before cutting off because of multiphonon absorption. This type of polarizer thus also fails to meet the high extinction and broad wavelength coverage requirements for a master infrared polarizer.

D. Transmissive Brewster's Angle Polarizers

Brewster's angle polarizers rely on the different transmission and reflection coefficients for *s*- and *p*-wave polarization at the interface between two materials. The light ray path for a dielectric plate is sketched in Fig. 2. The incident irradiance $(\epsilon_0/4\mu_0)^{1/2}(\mathbf{E}_s^2 + \mathbf{E}_p^2)$ is partially reflected and par-

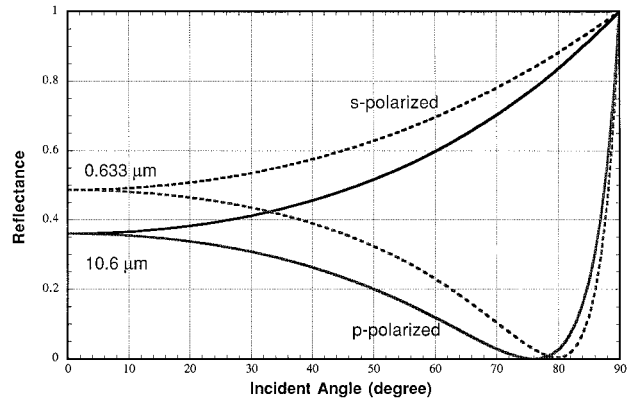


Fig. 3. Reflectances α and β for *s* and *p* wave, respectively, for the first surface of a vacuum germanium interface as a function of incident angle. These are shown for wavelengths of 10.6 μm (solid curve) and 0.633 μm (dashed curve). The 0.633- μm *p* wave does not quite reach zero ($\beta \approx 0.0038$ at 80°) at the minimum because of absorption. At 0.633 μm the complex index of refraction is given by $n \approx 5.5$ and $k \approx 0.7$.

tially refracted at the first surface. The subscripts *s* and *p* refer to electric-field vectors perpendicular and parallel, respectively, to the plane of incidence. The constant prefactor contains the permittivity ϵ_0 and permeability μ_0 of free space and assumes that the refractive index of the surrounding medium is 1. According to Fresnel theory, the first-surface reflected beam has irradiance $(\epsilon_0/4\mu_0)^{1/2}(\alpha\mathbf{E}_s^2 + \beta\mathbf{E}_p^2)$, where α and β are the reflectances for the *s* wave and *p* wave, respectively. When the angle of incidence θ is near Brewster's angle θ_B , β is nearly zero. That is, at Brewster's angle the *p* wave is entirely refracted at the first surface. In a beam with finite convergence (or divergence) the fraction β is nonzero because of the distribution of incidence angles about θ_B . Figure 3 shows the reflectances α and β for the first surface of a vacuum germanium interface as a function of incident angle. Over much of the infrared, the germanium refractive index of $n = 4.0$ and Brewster's angle $\theta_B = 76^\circ$. Two types of polarizers can be constructed with Brewster's angle—transmissive or reflective.

The transmissive Brewster's angle polarizer typically stacks m plates in a V geometry. The extinction ratio of refracted light through each interface is $(1 - \alpha/1 - \beta)$ and after $2m$ interfaces, the extinction ratio becomes

$$\rho = \frac{[(1 - \alpha)(1 + \beta)]^m}{[(1 + \alpha)(1 - \beta)]^m}. \quad (1)$$

Equation (1) sums multiple reflections in each plate, ignoring walk-off, absorption, and interference, and neglects multiple reflections between the plates. Four germanium plates in such a configuration yield an extinction ratio approximately 2×10^{-4} over a usable spectral range from 3 to 15 μm . Figure 4 shows the spectral major principal transmittance k_1 (*p* wave) of a single germanium plate at Brewster's

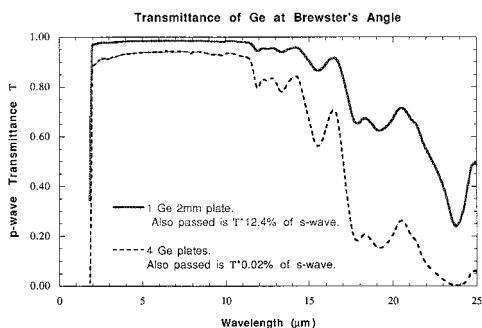


Fig. 4. *P*-wave transmittance of a single germanium plate at Brewster's angle (solid curve) and that raised to the fourth power to approximate the major principal transmittance k_1 of a four-plate transmissive Brewster's angle polarizer (dashed curve).

angle and that transmittance raised to the fourth power to approximate a four-plate device. A germanium transmissive Brewster's angle polarizer is spectrally featureless from approximately 2 to 12 μm , exhibiting a major principal transmittance $k_1 \sim 1$. Absorption does not permit use of the device below 1.8 μm . Because visible light is not transmitted, the device is difficult to align in an optical system. A similar ZnSe device can be used out to 14 μm and it will allow visible transmission. Interference of the reflected *s*-polarized radiation within and between the stacked Brewster plates can be a significant problem for well-collimated, monochromatic light. This can potentially yield order-of-magnitude variations in the extinction ratio with wavelength, angle of incidence, position, temperature, etc. Beam deviation depends on unintentional wedging in the plates and is typically less than 1 mrad.¹⁰ Acceptance angles are less than 100 mrad. Germanium transmissive Brewster's angle polarizers present an attractive potential for metrology because of the high quality and the broad infrared range of utility. The difficulty of alignment, potential interference problems, and the spectral range limitation led us to seek another polarizer type—the reflective Brewster's angle polarizer—for our metrology application.

E. Reflective Brewster's Angle Polarizers

For transparent dielectrics, the *p*-wave reflectance nulls at Brewster's angle. Ideally, a single-surface reflection provides complete extinction. However, significant spectral variation of the index of refraction and spectral regions of high absorption affect the *p*-wave reflectance. In the first case, variation of the index of refraction shifts the Brewster angle of the *p*-wave reflectance minimum. In the second case, high absorption shifts the *p*-wave reflectance minimum to a nonzero value. For germanium the real component of the index of refraction n is nearly 4 from the ultraviolet, rising to a maximum near 6 in the visible and is again nearly 4 far into the infrared. The complex component of the index of refraction k is approximately 2 from the ultraviolet, falling to nearly 0 in the near infrared and the far infrared. Brew-

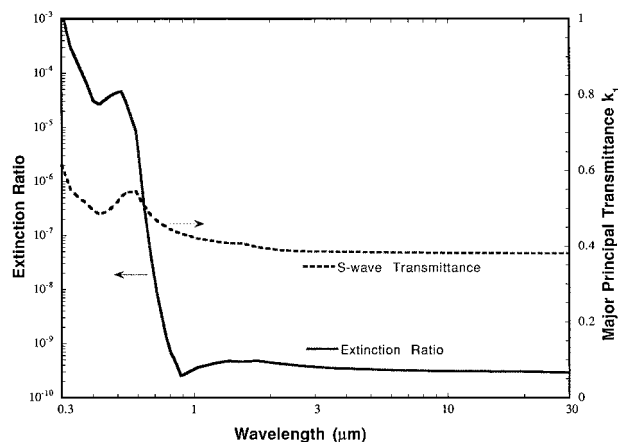


Fig. 5. Extinction ratio (solid curve) and major principal transmittance k_1 (dashed curve) calculated with Fresnel theory for four germanium plates reflecting at 76.5 deg. Only first-surface reflections are considered. The 0.22 sr ($f/14$) beam divergence used in the calculation limits the extinction ratio from achieving complete null. Though not shown, the curves extend nearly featurelessly to beyond 500 μm .

ster's angle does not significantly change so that difficulties from the first case are minimal. Only in the ultraviolet does the absorption in germanium become substantial enough to yield poor extinction performance because of incomplete null of the *p*-wave reflectance. Figure 5 displays the calculated extinction ratio and calculated major principal transmittance k_1 for a four-germanium plate device illuminated at Brewster's angle with a 35-mrad half-angle ($f/14$) beam. The chevron geometry considered for these germanium plates is sketched in Fig. 6(a). The calculations demonstrate that such a polarizer would be useful from 0.3 to 30 μm —over nearly the full spectral range of our spec-

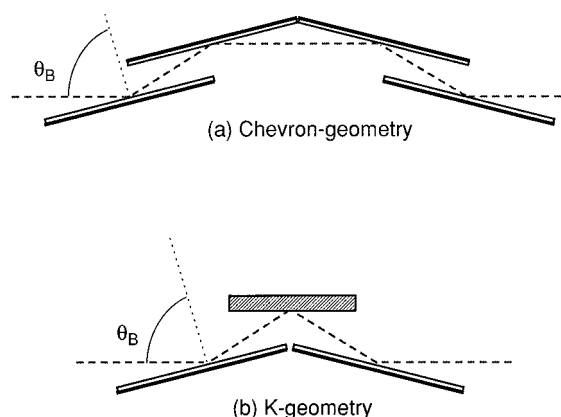


Fig. 6. (a) Sketch of the chevron geometry considered for the four germanium plates. There is no image inversion. (b) Basic *K*-geometry polarizer shown with two Brewster plates and one plane mirror. Because three reflections are involved there is image inversion. An off-center displaced input beam is displaced at the exit to be parallel but not collinear with the input. An angularly off-axis input beam is deviated angularly at the exit to be nonparallel with the input beam.

trometers. Such a polarizer should be useful at even longer wavelengths out to 500 μm . The calculated extinction ratio is less than 10^{-5} over nearly this entire range.

The calculated major principal transmittance k_1 is approximately 0.4 over this range. The acceptance half-angle is 70 mrad ($f/7$). Beam deviation can be less than 1 mrad, depending on construction accuracy. Beam displacement can be less than 0.5 mm, depending on construction accuracy and alignment. For our metrology needs we also required that the polarizers be robust, have collinear input and output beams, and be simple to align. On the basis of the expected performance, we designed, built, and tested reflective Brewster's angle polarizers for our metrology needs.

3. Device Design and Construction

In this section we describe a prototype of the reflective Brewster's angle polarizers, the final chevron polarizer design, and its construction. Two primary versions of the reflective Brewster's angle polarizer seemed to meet our needs: a chevron geometry version and a *K*-geometry version. The *K*-geometry polarizer^{11,12} is shown schematically in Fig. 6(b). Ideally, light reflects through the device (either version) in a symmetric path and exits collinear to the incoming beam.

To evaluate more easily the general performance characteristics of reflective Brewster's angle polarizers, we first constructed a prototype *K*-geometry polarizer with fused-silica plates and an aluminum mirror. A beam block was placed between the fused-silica plates to stop the *p*-wave flux transmitted through the first plate. The fused-silica *K*-geometry polarizer was tested with 0.633- μm wavelength light from a He-Ne laser, a pair of Glan-Taylor polarizers, and a silicon photodiode coupled to a polytetrafluoroethylene (PTFE) integrating sphere. Brewster's angle is 56° for fused silica at 0.633 μm . The extinction ratio initially measured was larger than expected. Multiple beams, at least three, were emitted from the fused-silica *K*-geometry polarizer. These were separated from one another by approximately 0.2 mrad. Two of these generated beams could not be completely extinguished by orienting the polarization axis of the incident beam. We determined that the multiple beams were generated by reflections from the back surface of the fused-silica plates. The beam deviation was consistent with unintentional wedging in the plates. We postulate that birefringence generated elliptically polarized light in these secondary beams. We replaced the original plates by fused-silica plates with a roughened back surface that was painted with black paint. This suppressed the back surface reflections. With only first-surface reflections, the fused-silica *K*-geometry polarizer extinction ratio was measured to be less than 5×10^{-5} .

The major principal transmittance k_1 was measured to be 0.013. The low value of the major principal transmittance k_1 results from the similarity of the indices of refraction of fused silica and air. This

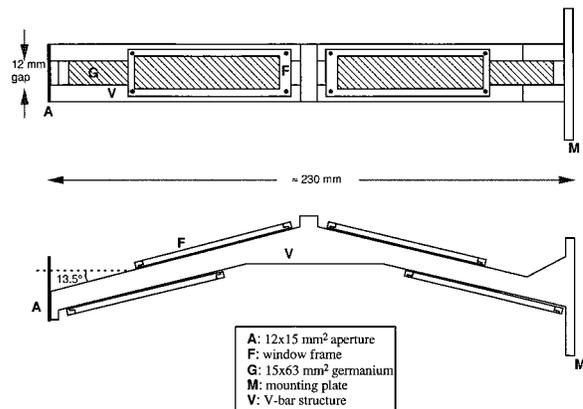


Fig. 7. Germanium chevron polarizer construction.

contrasts with more acceptable values of $k_1 \sim 0.4$, calculated for the four-plate germanium polarizer. The high value of the germanium index of refraction results in a tolerably high major principal transmittance. Lower-index materials would achieve lower values of the major principal transmittance k_1 .

The *K*-geometry polarizer inverts the input beam because of the three reflections. Brewster's angle is alignment insensitive; small deviations from the optimum angle yield only small values of the *p*-wave reflectance. However, tipping the input beam relative to the *K*-geometry polarizer optic axis deviates the output beam. In addition, displacing the input beam relative to the *K*-geometry polarizer optic axis displaces the output beam. These serious alignment effects do not exist in the chevron geometry polarizer.

We built two germanium chevron geometry polarizers. The germanium chevron geometry polarizer construction is shown in Fig. 7. The basic structure consists of two shallow V-shaped bars connected to one another by a mounting plate at one end and by cross members at the apex and at the other end. The bars are parallel to one another and have parallel faces inside and outside the V. These parallel faces orient the first surfaces of the germanium plates¹³ in the configuration depicted in Fig. 6(a). Four frames bolt onto the faces to hold the germanium plates flush to the inside and outside of the V bars as shown. The germanium plates straddle the gap between the V bars. The optical path follows between the two V-shaped bars. The basic structure was cut from a single block of 303 stainless steel with a wire electric discharge machine. We successively annealed and cut three times to achieve a single piece with the parallelism needed. The inside and outside V faces are parallel to less than 0.1 mrad. Between the back side of the germanium and the frame is a sheet of rubber that serves to cushion the germanium plate and to block transmitted infrared light. The mounting plate on one end is contiguous with the rest of the V-bar structure. A rectangular metal aperture bolts onto the other end of the V-shaped structure. A focal point at the polarizer optical center and the aperture limit the acceptance half-angle to be 3.5° .

The single-piece construction of the basic structure ensures that the polarizer will remain aligned so that the performance will be stable over a long time, even after repeated rotations on a motorized rotation stage. This structure was designed in the above manner to have no adjustments for the germanium plate orientation. This construction is practical both because the performance is insensitive to small deviations from Brewster's angle and because the nominally symmetric four-reflection path preserves image orientation. In contrast to the *K*-geometry polarizer, tipping the input beam relative to the chevron geometry polarizer optic axis only slightly displaces the output beam. As discussed below, the polarizer performance is limited by scattering, not by alignment. Displacing the input beam relative to the chevron geometry polarizer optic axis does not displace or deviate the output beam. Rotation of the polarizer, when aligned in an optical beam, results in an output beam deviation of at most 1 mrad. Alignment of the chevron polarizer in an optical system is quite simple and can be performed with visible light.

4. Germanium Chevron Polarizer Testing

The germanium chevron polarizers were tested extensively with four lasers—a 0.633- μm wavelength He–Ne laser, a 1.32- μm wavelength diode laser, a 3.39- μm wavelength He–Ne laser, and a 10.6- μm wavelength CO_2 laser. The testing included measurements of the extinction ratio and the major principal transmittance. The polarizer was also rotated in a polarized beam to check that the transmitted irradiance was proportional to $\cos^2 \theta$ (Malus's law), where θ is the rotation angle that the chevron polarization axis makes with respect to the beam's polarization. For most of the experiments, a laser was followed by a chopper, a high-quality polarizer, the polarizer under test, and a detector. Usually the detector signal was fed into a lock-in amplifier. The polarizers were mounted and aligned on motorized rotation stages with an angular resolution of 0.03 mrad. The lock-in amplifier output was read by a computer, and the motorized rotation stage angles were controlled by the computer.

Although ideally the measurements would be made in a perfectly polarized beam, this was not always practical. For the 3.39- μm wavelength laser experiments, a calcite polarizer was determined to be of such high quality, i.e., sufficiently lower extinction than the germanium chevron polarizers, that this ideal situation was approachable. For the 0.633- μm wavelength laser experiments, the Glan–Taylor polarizers were found to have extinction ratios similar to the germanium chevron polarizers. For the 1.32- μm and 10.6- μm measurements, no available polarizer approached the extinction ratios of the germanium chevron polarizers. Therefore, for the 0.633-, 1.32-, and 10.6- μm wavelength laser experiments, two germanium chevron polarizers were used in series. The polarizers were assumed to be identical, and we calculated the extinction ratio by measuring the crossed pair transmittance $H_{90} = k_1 k_2$ and

the parallel pair transmittance $H_0 = \frac{1}{2}(k_1^2 + k_2^2)$ in a nominally unpolarized beam. From these quantities, the extinction ratio can be given by

$$\rho = \frac{\sqrt{H_0 + H_{90}} - \sqrt{H_0 - H_{90}}}{\sqrt{H_0 + H_{90}} + \sqrt{H_0 - H_{90}}} \approx \frac{H_{90}}{2H_0}. \quad (2)$$

The approximation in Eq. (2) holds in the limit as the extinction ratio approaches zero. We measured the major principal transmittance by setting the second polarizer to the angle for maximum, parallel pair transmittance and then removing the polarizer from the beam. Except for the 10.6- μm experiments, signal drift over the time scale needed to remove the polarizer was typically less than 0.5%. The following subsections describe the specific details for the measurements at the four different laser wavelengths.

A. Laser Experiments at the 0.633- μm Wavelength

The almost randomly polarized output beam of the 0.633- μm wavelength He–Ne laser was collimated within a beam divergence of less than 0.2 mrad. Corrections were made to Eq. (2) to account for the slight linear polarization of the beam. The detector used for these experiments was a 10-mm-square silicon photodiode. The Si photodiode was coupled to a transimpedance amplifier that amplified the photocurrent to a voltage that was subsequently coupled to the lock-in amplifier. Similar photodiodes operated in this photocurrent mode have demonstrated as much as 14 decades of linearity.¹⁴ This photodiode was mounted to the exit port of a PTFE-integrating sphere. The 6-mm-diameter sphere entrance port presented a polarization and position-insensitive detection aperture that was underfilled by the beam in these experiments. Two germanium chevron polarizers mounted on rotation stages were placed in this beam, and the rotation angle θ for the second polarizer was varied for measurement of the crossed pair transmittance H_{90} , the parallel pair transmittance H_0 , and the $\cos^2 \theta$ dependence. We checked the lock-in amplifier zero level by blocking the laser and we subtracted this from the detector signal for these measurements.

B. Laser Experiments at the 1.32- μm Wavelength

The polarized output beam of the 1.32- μm -wavelength diode laser was collimated by a lens integrated onto the laser head. The beam divergence was approximately 10 mrad. The detector used for these experiments was a thermoelectrically cooled 10-mm-diameter InGaAs photodiode. The InGaAs photodiode was integrated with a transimpedance preamplifier that was coupled subsequently to the lock-in amplifier. Operated in the photocurrent mode, this photodiode is also expected to be highly linear. No integrating sphere was used; the beam was focused to underfill the 10-mm-diameter InGaAs. The polarization axis of the first germanium chevron polarizer was oriented at 45° to the polarization axis of the 1.32- μm wavelength diode laser's

chopped beam. An intermediate aperture was placed between the laser and the first polarizer to limit the beam size to be smaller than the polarizer acceptance aperture. Again the rotation angle θ for the second germanium chevron polarizer was varied for measurement of the crossed pair transmittance H_{90} , the parallel pair transmittance H_0 , and the $\cos^2 \theta$ dependence. For the 0.633- μm and 1.32- μm light the germanium plates were opaque; therefore the reflections from the second surface within each Ge plate were suppressed.

C. Laser Experiments at the 3.39- μm Wavelength

The polarized output beam of the 3.39- μm wavelength He-Ne laser was nearly collimated. An aperture after the laser limited the beam size. The beam divergence was approximately 4 mrad. The detector used for these experiments was a 0.5-mm-diameter InSb detector operated at 77 K. The InSb detector was coupled to the lock-in amplifier with an audio transformer. No integrating sphere was used; the beam was focused with a lens to underfill the InSb detector. The He-Ne laser's polarized beam was followed by a quarter-wave plate oriented to produce a circularly polarized beam. When a single polarizer was rotated 360° in this circularly polarized beam, the detector signal output varied by less than a few percent. Two dichroic calcite polarizers (each 2 mm thick) were placed in this beam, and the extinction ratio for one of these was measured to be $\rho \sim 3 \times 10^{-8}$. When measuring the two polarizers in the parallel configuration, we placed a filter with transmittance $T = 0.0089$ in the beam to avoid saturation and to ensure linearity of the detector. When measuring the two polarizers in the crossed configuration, we removed the filter from the beam.

The second of these dichroic calcite polarizers was then replaced with the germanium chevron polarizer under test. Because the extinction ratio of the preceding dichroic calcite polarizer is so low, the chevron polarizer is tested in a more nearly ideal polarized beam. The extinction ratio of the germanium polarizer k_2 is determined from the measured intensity ratio $H_{90}/H_0 = (k_1 + k_2)/(1 + k_1k_2)$, which holds for two polarizers in series in an unpolarized incident beam. Because the extinction of the calcite polarizer is ten times lower than the Ge polarizer, the difference between the measured intensity ratio and the actual Ge polarizer extinction is approximately only 10%. Again, the rotation angle θ for the germanium chevron polarizer was varied for measurement of the major principal transmittance k_1 , minor principal transmittance k_2 , and the $\cos^2 \theta$ dependence. The filter was used again for the measurement of H_0 .

D. Laser Experiments at the 10.6- μm Wavelength

The polarized output beam of the 10.6- μm wavelength CO₂ laser was limited by an aperture and a filter. The beam divergence was approximately 4 mrad. Two detectors were used for these experiments—a liquid-nitrogen-cooled, 3-mm-diameter HgCdTe detector and a 14 mm \times 14 mm square pyroelectric detector.

The HgCdTe detector was more sensitive, but the laser was powerful enough that the less-sensitive pyroelectric detector could also be used. No integrating sphere was used; the beam was focused to underfill the detector, but position sensitivity in combination with beam displacement was a major contributor to measurement uncertainties. The extinction ratio was measured with the HgCdTe detector. A filter was used to measure the parallel pair transmittance H_0 ; no filter was used to measure the crossed pair transmittance H_{90} . The major principal transmittance k_1 was measured with the pyroelectric detector. The CO₂ laser's polarized beam was oriented at 45° to the first germanium chevron polarizer as was done in the 1.32- μm wavelength diode laser experiments. Again, the rotation angle θ for the germanium chevron polarizer was varied for measurement of the $\cos^2 \theta$ dependence.

For both the 0.633- μm and the 1.32- μm light, the germanium plates are opaque. But for both the 3.39- μm and the 10.6- μm light, the germanium plates are transparent; reflections from the second surface within each germanium plate are not attenuated. Therefore interference effects and multiple beams are possible. At Brewster's angle, a front/back surface wedging of 0.05° in a Ge plate deviates the second-surface reflected beam 1.8° from the first-surface reflected beam. The second-surface reflection can be suppressed either by volume absorption, intentional wedging, second-surface roughening to induce diffuse scattering, and/or second-surface coating to induce absorption. Another effect of transmission in the germanium is that the p -wave transmittance through the first and fourth plates may allow the rubber sheet (behind the Ge) material transmittance to contribute to the minor principal transmittance. At 3.39 μm the rubber sheet is opaque, but at 10.6 μm the rubber sheet transmittance is approximately 10^{-4} .

E. Measurements of the ϕ -Dependence of the Transmittance

In all four laser configurations, the polarizer under test was rotated about the optical axis in the polarized beam while we monitored the signal. Figure 8 shows the detector signal measured at 1.32 μm as a function of the rotation angle θ . This displays the expected $\cos^2 \theta$ behavior. Because the germanium plates are opaque at 0.633 and 1.32 μm , the response to a similar measurement at 0.633 μm yields a similar result.

Figure 9 shows the detector signal measured at 3.39 μm as a function of the rotation angle θ . The dotted curve shows the first data taken when the parallel germanium plates were unaltered. The structure in the curve does not result from beam wander off the detector while rotating. Rather, the structure in the curve results from interference with respect to the first and second surface reflections in the plates. As the polarizer is rotated, slight misalignment causes different optical path lengths within the plates. Constructive or destructive inter-

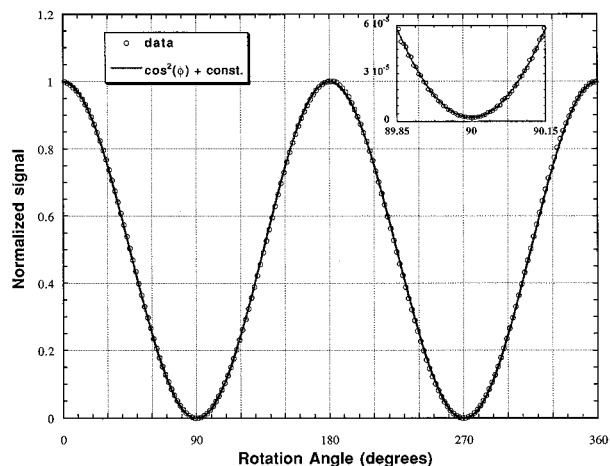


Fig. 8. Detector signal (open circles) measured at $1.32 \mu\text{m}$ and the ideal $\cos^2 \phi$ (solid curve) as a function of the rotation angle ϕ . The inset shows the minimum of the data.

ference was allowed for these different path lengths for any of the plates. Only at the null orientation, when the p wave is not reflected from either surface, is the interference nonexistent. The measured curves were generally not reproducible if any realignment had occurred. However, the null value was reproducible. In these conditions the maximum signal is not well reproduced; only an estimate of the major principal transmittance k_1 and the extinction ratio could be made. Because the germanium plates are transparent at 3.39 and $10.6 \mu\text{m}$, the response to a similar measurement at $10.6 \mu\text{m}$ yields similar interference effects.

To suppress the second-surface reflection, we attempted to absorb radiation at the second surface by coating it with a black, graphite-loaded epoxy.¹⁵ If

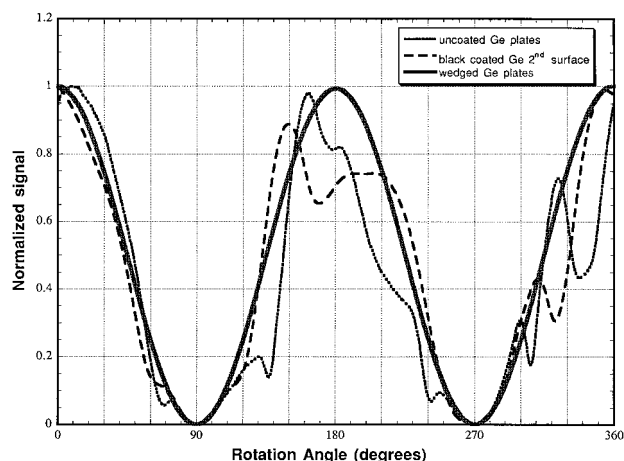


Fig. 9. Detector signal measured at $3.39 \mu\text{m}$ as a function of the rotation angle θ . We obtained the dotted curve data using the uncoated germanium plates in the polarizer. The dashed curve data were obtained when we used the germanium plates with the back surface painted black. The solid curve data were obtained with use of the wedged germanium plates and are nearly indistinguishable from the ideal $\cos^2 \theta$ (not shown).

the radiation were absorbed at the blackened second surface, no reflected beam would exist to interfere with the first-surface reflected beam. This is similar to the technique we used in the fused-silica K -geometry polarizer prototype. The dashed curve in Fig. 9 shows the data taken when the germanium second surfaces were epoxy-coated black. The interference structure is not sharply structured as in the previous parallel uncoated case, but it is not eliminated. The black graphite-loaded epoxy did not absorb sufficiently to quench the interference effects. This is probably because the poor match between the high index of refraction of germanium and the index of refraction of the black graphite-loaded epoxy; so the reflectance at the interface is still appreciable.

To quench more completely the interference from the second-surface reflections, we intentionally wedged the germanium plates. We chose a 1° wedge angle in the optical plane of incidence. The steel V bars of the chevron construction still defined the first-surface orientation at Brewster's angle. But the second surface was now no longer at Brewster's angle but rather at an angle greater than the critical angle for total internal reflection. Subsequent reflections were internal reflections. The internal rays ideally reflect multiple times to the end and reflect back, exiting in the backward direction. The solid curve in Fig. 9 shows the data taken when the germanium plates were intentionally wedged. Again, these data are very nearly the $\cos^2 \theta$ curve. The data were quite reproducible; reliable measurements of the major principal transmittance k_1 and the extinction ratio could be made.

For a perfect wedge, the radiation meanders back and forth and is ultimately backscattered. Our wedges have cut but unpolished ends. These unpolished ends, surface imperfections, and volume defects all tend to scatter the internally reflected light in directions other than in the backward direction. However, the amount of scattering in the detector acceptance cone is small. The internal path length for these reflections can be more than 100 mm so absorption is more likely. Intentionally doping the germanium may help if absorbing the scattered radiation is important. Although wedging the plates in another direction is also feasible, the performance suffices with this wedging. The extinction ratio was lower (Table 1) than in the parallel and epoxy-coated germanium plate cases.

F. Extinction Ratio and the Major Principal Transmittance

Table 1 shows the extinction ratio ρ and the major principal transmittance k_1 of the germanium chevron polarizers at the four laser wavelengths. The results at $3.39 \mu\text{m}$ are shown for three different cases: the parallel plates, the plates with the second surface epoxy-coated black, and the wedged plates. The extinction ratio and principal transmittances for wavelengths below $1.8 \mu\text{m}$, where the germanium is opaque, are unaffected by the wedging of the plates. Misalignment and scattered radiation always tend to yield a higher value of the extinction ratio. We ob-

Table 1. Extinction Ratio ρ and the Major Principal Transmittance k_1 of the Germanium Chevron Polarizers at the Four Laser Wavelengths

Laser Wavelength	Germanium Plates Installed in Polarizer	Extinction Ratio ρ		Major Principal Transmittance k_1	
		Calculated	Measured	Calculated	Measured
0.633- μm He-Ne	Uncoated second surface	3.7×10^{-7}	$4.0 \times 10^{-6} \pm 0.8 \times 10^{-6}$	0.51	0.50 ± 0.02
1.32- μm diode	Uncoated second surface	4.8×10^{-10}	$1.5 \times 10^{-7} \pm 0.4 \times 10^{-7}$	0.41	0.40 ± 0.02
3.39- μm He-Ne ^a	Uncoated second surface	3.6×10^{-10}	$1.2 \times 10^{-5} \pm 0.3 \times 10^{-5}$	0.38	0.60 ± 0.15
3.39- μm He-Ne ^a	Blackened second surface	3.6×10^{-10}	$2.0 \times 10^{-4} \pm 0.5 \times 10^{-4}$	0.38	0.60 ± 0.15
3.39- μm He-Ne	Wedged Ge plates	3.6×10^{-10}	$3.3 \times 10^{-7} \pm 0.5 \times 10^{-7}$	0.38	0.37 ± 0.01
10.6- μm CO ₂	Wedged Ge plates	3.1×10^{-10}	$3.0 \times 10^{-8} \pm 0.6 \times 10^{-8}$	0.38	0.35 ± 0.05

^aThe data in this row were compromised by interference problems rectified by wedging the germanium plates.

tained the measured extinction ratios shown in the table after performing the measurements with various-sized apertures at the source or detector and realigning the measurement system. The expanded uncertainties¹⁶ shown in the table are estimated from this aperturing and realignment. In general, the measured extinction ratio was always larger for larger apertures. The extinction ratios measured at the laser wavelengths all fall above the extinction ratios of the Fresnel calculations. Although the 0.633- μm measured extinction ratio is close to the calculated extinction ratio, the other measured extinction ratios are well above the calculated extinction ratios. The discrepancy is significantly above the noise limitation for these measurements.

We surmise that the measured extinction ratio does not achieve the Fresnel calculated performance because light scatters from imperfect first surfaces of the germanium plates into the detector. A calculation¹⁷ was made of the amount of light scattered into the acceptance cone of the detector. We assumed a surface roughness similar to that found on silicon wafers for this calculation. The scattering estimation would give a result of the order of 10^{-8} for the extinction ratio. The surface quality is quite likely not as good as that for silicon wafers so this is an underestimation of the extinction ratio limited by scattering. The measurements of the extinction ratio are also an upper bound because scatter off the V-bar construction or any of the other optical components contributes to the signal. This is not uncommon at the 10^{-8} level.

Another possible contributor to light scattering in the polarizers is dust or other surface particles on the Ge plates. The polarizers have not been kept in a clean room environment, but were covered with plastic and stored in a purged enclosure when not in use. We do not believe that dust is the dominant source of scattering, because cleaning the surfaces with alcohol and lens tissue and dusting with dry nitrogen did not have a noticeable effect on the measured extinction. Microscopic examination of the Ge plates at moderate magnification (30 \times) revealed some scratches and pits from the polishing process, but no noticeable particles. However, we plan to perform bidirectional reflectance distribution function measurements on at least one wedged Ge plate to characterize the distri-

bution of scattered light from both the front surface and the internal reflections.

The major principal transmittances measured at the laser wavelengths agree with the values of the Fresnel calculations. Only the results at 3.39 μm shown for the first two cases of the parallel plates and of the plates with the second surface epoxy-coated black are not reliable because of the above-mentioned interference problems. These two cases yield measured major principal transmittance k_1 values greater than expected from the Fresnel calculations. This corroborates our interpretation of interference difficulties in these two geometries; the excess of the major principal transmittance results from constructive interference. For the wedged plate geometry, the agreement of the measured values of the major principal transmittance k_1 with the Fresnel calculations at 3.39 and 10.6 μm confirms that the wedged plates correct the interference problems. The expanded uncertainties of the measured major principal transmittance also stem from the alignment repeatability of removing and replacing the polarizer in the optical beam. For the 10.6- μm wavelength laser measurements, the laser drift over the time scale of removing and replacing the polarizer in the optical beam contributes significantly to the major principal transmittance measurement uncertainty.¹⁸

5. Discussion

The interference problems encountered in the transparent spectral range of the germanium were evident from the $\cos^2 \theta$ experiments. For parallel plates of thickness t and index n irradiated at a wavelength λ , these interference problems are expected only from monochromatic sources where the fractional bandwidth $\delta\lambda/\lambda$ obeys

$$\frac{\delta\lambda}{\lambda} < \frac{\lambda}{nt}. \quad (3)$$

We suppressed the interference problems in the Brewster's angle germanium chevron polarizers by wedging the plates. We expect that similar interference problems may be encountered with other slab geometry polarizers used with narrow-band sources. We may need to limit the resolution of our spectrometers to avoid these problems when measuring other

Table 2. Summary of the Major Performance Parameters of the Germanium Chevron Polarizers and Other Polarizer Types

Polarizer Type	Wavelength Range (μm)	Extinction Ratio ρ	Major Principal Transmittance k_1
Dichroic polymer sheet	0.4–0.8	10^{-2} – 10^{-3}	0.6–0.7
Dichroic metal particles in glass	0.9–1.7	10^{-2} – 10^{-5}	0.8–0.9
Dichroic calcite crystal	3.35–3.45	10^{-8} – 10^{-9}	0.7–0.8
Wire grid	2–15	10^{-1} – 10^{-3}	0.5–0.9
Glan prism	0.3–2.2	10^{-4} – 10^{-5}	0.6–0.8
Ge transmissive Brewster's angle	2–15	10^{-3} – 10^{-4}	0.5–0.99
Ge chevron-reflective Brewster's angle	0.4–50	10^{-5} – 10^{-7}	0.4–0.5

polarizer types. If interference is suspected, the polarizer should be rotated in a polarized beam to check for the $\cos^2 \theta$ dependence.

The choice of germanium as the reflecting material for the Brewster's angle chevron polarizers was dictated by the high and nearly constant index of refraction over the broad wavelength range. The high index of refraction yields a satisfactory value for the major principal transmittance. A similar device of glass or fused silica would have a major principal transmittance k_1 of only 10^{-4} .

The germanium chevron polarizers have not yet been tested over the entire spectral range. We plan to measure the spectral extinction ratio and major principal transmittance of the germanium chevron polarizers. Preliminary measurements indicate that, over much of the intended spectral range, the extinction ratio is lower than our spectrometers can measure. This is partly because of the small étendue of the polarizers. This would not be a problem if the polarizers were scaled up.

We will measure the spectral extinction ratio and major principal transmittance of some of the dichroic, wire grid, and Glan polarizers by incorporating the germanium chevron polarizers into our spectrometers for spectral polarimetry. We plan to repeat some laser-based measurements similar to those described in this paper on these other polarizer types.

6. Summary

We have described new reflective Brewster's angle polarizers using germanium plates in a chevron geometry for visible and infrared metrology uses. Their performance has been presented in the context of other polarizer types. Table 2 summarizes the performance parameters of the germanium chevron polarizers and the other polarizer types discussed. The major parameters presented in the table are the wavelength range of operation, the extinction ratio, and the major principal transmittance. From the table it is evident that the reflective Brewster's angle polarizers can be used over the range of our spectrom-

eters as master polarizers for characterizing the other types of polarizers.

The robust construction of the chevron geometry polarizer satisfies many of our metrology goals. The ability to align the polarizers with visible light and the insensitivity to slight misalignment are significant advantages over other Brewster's angle polarizers. However, the Brewster's angle chevron geometry polarizer may be cumbersome for some applications in which a compact, slab geometry is more desirable. The Brewster's angle chevron geometry polarizer offers the further metrology advantage that the polarization direction of the beam exiting the polarizer is unambiguously defined. By retroreflecting a beam off one of the plates, the plane of the extinguished p wave can be located accurately. This feature can be used to define the polarization axis of other polarizers that could be calibrated with the chevron geometry polarizers.

Appendix A

The literature is somewhat divided on the definition of the extinction ratio. Our definition of k_2/k_1 as measured by exposure to linearly polarized light follows the Commission Internationale de l'Eclairage definition⁵ and that of other authors.^{18–20} A second set of authors^{21,22} define the extinction ratio to be H_{90}/H_0 as measured by crossing two identical polarizers exposed to unpolarized light. A third set of authors^{12,23,24} refer to its inverse, k_1/k_2 or similar quantities as the extinction coefficient or extinction ratio. Our preference against the inverse definition (third set of authors) stems in part from linguistics—we believe full extinction should approach zero, in analogy to the biological usage. However, our preference against the inverse definition is largely practical. For extremely low minor principal transmittance k_2 , detector noise and stray light errors contribute only minimally to the extinction ratio of our definition but contribute enormously to the inverse definition. We refer to the inverse of the extinction ratio as the contrast ratio.

Our preference against the definition of the extinction ratio as H_{90}/H_0 is more subtle. We believe it is difficult to verifiably produce an unpolarized beam and to trust the similarity of a pair of polarizers. These are the prerequisites for measurement of H_{90}/H_0 . Rather, it is often more practical to find a polarizer of negligible k_2 to act as a generator of polarized light. This is the prerequisite for the measurement of the major and minor principal transmittances k_1 and k_2 . In practice, our preferred definition and the definition of the second set of authors often differ by a factor of approximately 2. For many of the chevron polarizer measurements, another polarizer type of negligible k_2 was unavailable. Therefore our measurement technique was often similar to that proposed by the second set of authors, taking into account the factor of 2.

We thank the U.S. Navy for supporting this research as part of the metrology efforts of the Calibration Co-

ordination Group. We are grateful to T. Germer of the National Institute of Standards and Technology Optical Technology Division for performing the scattering calculation on the basis of his experience with silicon wafers for the semiconductor industry. A. Artau of Purdue University assisted in the measurements of the K -geometry prototype. We commend the enormous efforts of Dwight Berry and Dana Strawbridge of the machine shop at the National Institute of Standards and Technology in constructing the chevron polarizers to our demanding specifications.

References and Notes

1. L. Mattsson, "A focussing VUV-polarizer for valence electron spectroscopy. Design considerations," Uppsala University Institute of Physics Report UUIP-984 (Uppsala University, Uppsala, Sweden, 1978).
2. L. Mattsson, B. Wannberg, H. P. Veenhuizen, I. Reineck, and K. Siegbahn, "A focussing VUV-polarizer system for valence electron spectroscopy. Performance and test results," Uppsala University Institute of Physics Report UUIP-1009 (Uppsala University, Uppsala, Sweden, 1979).
3. L. Karlsson, L. Mattson, R. Jadrny, K. Siegbahn, and K. Thimm, "Valence electron spectroscopy using polarized He I radiation," *Phys. Lett. A* **58**, 381–384 (1976).
4. G. Rosenbaum, B. Feuerbacher, R. P. Godwin, and M. Skibowski, "Measurement of the polarization of extreme ultraviolet synchrotron radiation with a reflecting polarimeter," *Appl. Opt.* **7**, 1917–1920 (1968).
5. *Polarization: Definitions and Nomenclature, Instrument Polarization*, CIE Publication 59 (Commission Internationale de l'Éclairage, Paris, 1984). This standards committee document received special weight in our preference of notation.
6. J. Shumaker, "Self-study manual on optical radiation measurements. Part I - Concepts," Natl. Bur. Stand. (U.S.) Tech. Note 910-3 (U.S. GPO, Washington, D.C., 1977), Chap. 6.
7. Sensitivity to beam convergence and input angle are almost always asymmetric because of the necessary asymmetry of the polarizing mechanism. Typically, we refer to the most restrictive angle when quantifying this.
8. Corning Incorporated, Corning, New York, 14831. One version of this type of polarizer is manufactured under the trade name Polarcor.
9. T. J. Bridges and J. W. Kluver, "Dichroic calcite polarizers for the infrared," *Appl. Opt.* **4**, 1121–1125 (1965).
10. II-VI Incorporated, Saxonburg, Pa. 16056. The PAZ and PAG polarizers consist of six plates of ZnSe and germanium, respectively.
11. L. J. Terminello, A. B. McLean, A. Santoni, E. Spiller, and F. J. Himpfel, "Low-pass filter for soft x-ray monochromators," *Rev. Sci. Instrum.* **61**, 1626–1628 (1990).
12. K. Rabinovitch, R. Canfield, and R. P. Madden, "A method for measuring polarization in the vacuum ultraviolet," *Appl. Opt.* **4**, 1005–1010 (1965).
13. Janos Technology, Incorporated, Townsend, New York 05353-7702. The germanium plates were specified to parallelism within 3 arc min.
14. G. Eppeldauer and J. E. Hardis, "Fourteen-decade photocurrent measurements with large-area silicon photodiodes at room temperature," *Appl. Opt.* **30**, 3091–3099 (1991).
15. Stycast 2850 FT epoxy, Gray Specialty Polymers, E. Z. Roberts and Associates, Culver City, Calif. 90232.
16. These are type B uncertainties. We determined the expanded uncertainty by multiplying the combined standard uncertainty by 2. B. N. Taylor and C. E. Kuyatt, "Guidelines for evaluating and expressing the uncertainty of NIST measurement results," Natl. Inst. Stand. Technol. Tech. Note 1297 (1994).
17. T. Germer, Optical Technology Division, National Institute of Standards and Technology, Gaithersburg, Md. 02889 (personal communication, 1997).
18. J. M. Bennett, "Polarization," in *Handbook of Optics 1*, M. Bass, ed. (McGraw-Hill, New York, 1995), Chap. 5.
19. *Optics and Filters Oriol Corporation Catalog 3* (Oriol Corporation, Stratford, Conn., 1990).
20. E. Collett, *Polarized Light* (Marcel Dekker, New York, 1993).
21. *Optics Guide 5: The Melles-Griot Catalog* (Melles-Griot, Irvine, Calif., 1990).
22. D. Kliger, J. Lewis, and C. Randall, *Polarized Lights in Optics and Spectroscopy* (Academic, San Diego, Calif., 1990).
23. *The Newport Catalog* (Newport Corporation, Irvine, Calif., 1994); D. O'Shea, *Elements of Modern Optical Design* (Wiley, New York, 1985).
24. R. Chipman, "Polarimetry," in *Handbook of Optics 2*, M. Bass, ed. (McGraw-Hill, New York, 1995), Chap. 22.